International Journal of Geosynthetics and Ground Engineering (2022) 8:46
https://doi.org/10.1007/s40891-022-00390-2

TECHNICAL NOTE

Determining Seismic Bearing Capacity of Footings Embedded in Cohesive Soil Slopes Using Multivariate Adaptive Regression Splines

Van Qui Lai[1,2] · Fengwen Lai[3] · Dayu Yang[3] · Jim Shiau[4] · Wittawat Yodsomjai[5] · Suraparb Keawsawasvong[5]

Received: 10 May 2022 / Accepted: 30 June 2022

Abstract

Seismic bearing capacity of strip footings in cohesive soil slopes considering various embedded depths is investigated in this study. Novel solutions using pseudo-static method and finite element limit analysis (FELA) with upper bound (LB) and lower bound (LB) theorems are presented. The influences of footing depth, slope angle, slope height, undrained shear strength and pseudo-static acceleration on bearing capacity and failure mechanisms are examined using dimensionless parameters. With the comprehensive numerical results, the multivariate adaptive regression splines (MARS) model is then utilized to simulate the sensitivity of all dimensionless input parameters (i.e., the normalized depth of footing *D/B,* the normalized slope height *H/B*, the normalized distance from top slope to edge of the footing *L/B*, slope angle β, the strength ratio $c_u/\gamma B$, and the pseudo-static acceleration factor, k_h). The degree of influence of each design parameter is produced, and an empirical equation for the dimensionless output parameter (i.e., bearing capacity factor N_c) is proposed. The study results are accessible in the design charts, tables, empirical equation for design practitioners.

Keywords Bearing capacity · Footing on slope · Pseudo-static · Seismic · Finite element limit analysis · MARS

Introduction

One of the most commonly used foundations in constructing railway tracks, retaining walls, transmission towers, and bridge piers is the strip foundation. These buried structures are typically supported by transferring their load to soils with enough bearing capacity and acceptable settling properties. Since the strip footing stability plays a significant role in practice, several researchers have considered the stability of strip footings on slopes by determining solutions from many different techniques including semi-empirical methods (e.g., [1–3]), limit equilibrium techniques (e.g., [4–7]), slip-line solutions (e.g., [8, 9]), limit analysis (e.g., [10–13]), finite element methods (e.g., [14–17]), finite element limit analysis [18], and discontinuity layout optimization (DLO) approaches [19–21]. However, there are a few works to study the influence of seismic events on the bearing capacity of footings on slopes, which should be a concern in earthquake areas due to the destructive effects of the footing during seismic situations. One conventional and widely used approach for determining the stability of embedded structures is the

✉ Suraparb Keawsawasvong
ksurapar@engr.tu.ac.th

Van Qui Lai
lvqui@hcmut.edu.vn

Fengwen Lai
laifengwen@163.com

Dayu Yang
220203414@seu.edu.cn

Jim Shiau
jim.shiau@usq.edu.au

Wittawat Yodsomjai
wittawat_yod@outlook.com

1 Faculty of Civil Engineering, Ho Chi Minh City University of Technology (HCMUT), 268 Ly Thuong Kiet Street, District 10, Ho Chi Minh City, Vietnam

2 Vietnam National University Ho Chi Minh City (VNU-HCM), Linh Trung Ward, Thu Duc District, Ho Chi Minh City, Vietnam

3 Institute of Geotechnical Engineering, Southeast University, Nanjing 211189, China

4 School of Engineering, University of Southern Queensland, Toowoomba 4350, QLD, Australia

5 Department of Civil Engineering, Thammasat School of Engineering, Thammasat University, Pathum Thani 12120, Thailand

Published online: 19 July 2022

pseudo-static approach, where the seismic forces are simply considered as horizontal and/or vertical seismic coefficients (k_h and k_v) and functions of gravity acceleration.

The seismic responses of a footing on soil have been one of important issues in geotechnical engineering [22–24]. Several research have been conducted to calculate the bearing capacity of strip footings on slopes with pseudo-static seismic forces considerations. The theoretical approaches, including limit equilibrium methods (e.g., [25–27]), lower bound solutions (e.g., [28]) and upper bound solutions (e.g., [29–33]), and the stress characteristic method (e.g., [34]) which delivered an effective solution to evaluate the problems. In comparison to the analytical techniques discussed previously, a prior assumption regarding the failure mechanisms is not required, therefore, it can provide excellent predicted performance with a wide range of parameters considered. Shiau et al. [35] and Raj et al. [36] investigated the seismic bearing capacity of sloped footings by employing finite element limit analysis (FELA) which provided the upper and lower bounds solutions.

By utilizing the lower bound FELA, Kumar and Chakraborty [37] also computed the bearing capacity factor N_g for a rough strip footing in cohesionless slopes under seismic scenarios. Subsequently, Chakraborty and Kumar [38] and Chakraborty and Mahesh [39] have studied the seismic bearing capacity of strip footings on a sloping ground surface and embankments utilizing the same methodologies. Using the Discontinuity layout optimization (DLO) technique, Zhou et al. [21] studied the ultimate seismic bearing capacity and failure mechanisms for strip footings placed close to the cohesive-frictional soil slopes. In addition, Cinicioglu and Erkli [40] investigated the seismic bearing capacity of strip footings lying on or adjacent to a slope by employing the finite element program PLAXIS in undrained conditions. Recently, the FELA technique was employed by Luo et al. [41], Beygi et al. [42], and Zhang et al. [23] to solve the seismic bearing capacity of strip footings on cohesive and cohesive-frictional soils, in spite that their solutions are limited to the cases of footings resting on the surface of slopes. Due to its popularity, the FELA technique has also been used to many other geotechnical problems [43–53].

In this paper, rigorous solutions of seismic bearing capacity of strip footing in cohesive soil slope are investigated by employing the finite element limit analysis (FELA) and a pseudo-static technique to evaluate the seismic loadings. The upper bound (UB) and lower bound (LB) outcomes attained by the FELA are compared with previously published results. The influences of the seismic acceleration coefficient, soil characteristics, and geometrical parameters on the seismic bearing capacity and the associated failure mechanisms of this problem are investigated. A comprehensive set of design tables and charts are also provided for the uses in design practices. The associated sensitivities are further assessed using multivariate adaptive regression splines (MARS) model, which is capable of accurately capturing the nonlinear relationships between a set of input variables and output variables in multi-dimensions. The MARS-based design equations used for forecasting the solutions of the seismic bearing capacity of strip footings embedded in cohesive slope are finally proposed using the artificial data set generated from FELA. The MARS-based design equation of the current study may be used to perform more precise and reliable evaluations of the seismic bearing capacity of this problem, while considering the coupled influences of the seismic acceleration coefficient, soil characteristics, and geometrical configurations.

Problem Statement and Modelling Technique

The problem definition of a strip footing on a slope is shown in Fig. 1. Under plane strain conditions, the slope has an inclination (β) and a height (H). The footing is assumed to be rigid material with width (B), depth (D), and the distance from top slope to edge of the footing (L). Defining the soil to

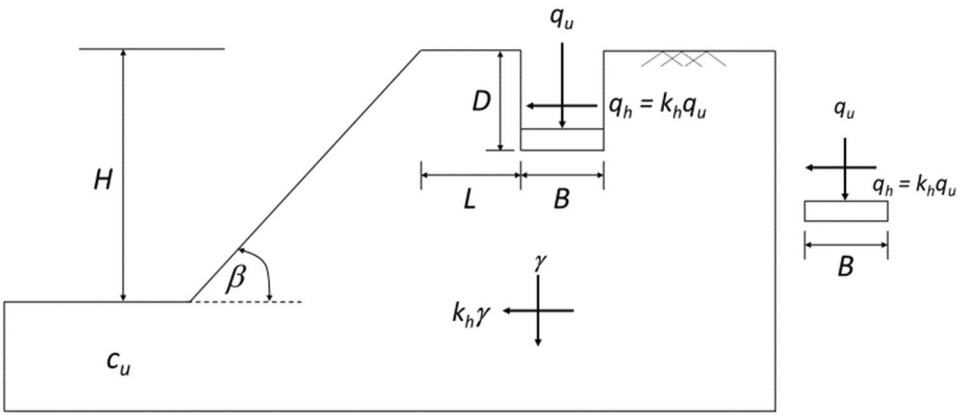

Fig. 1 Schematic diagram of the model

be a rigid-perfectly plastic Tresca material with a unit weight (γ) and undrained shear strength (c_u), the horizontal seismic acceleration (k_h) is applied to the footing and the slope under seismic forces. The vertical seismic acceleration is ignored in this study.

A typical model of the footing on slope problem is shown in Fig. 2. The boundary condition is determined using the standard fixity tool in OptumG2 [54], in which all boundary conditions are created as follows: both left-hand and right-hand boundaries are kept stationary in the x direction and the bottom of the boundary is fixed in both x and y directions. The movements at other boundaries are set to be freely moved in both x and y directions. The footing is model as a rigid elastic material and the footing-soil interface is considered as a perfectly rough condition. The size of the domain of this problem is chosen to be sufficiently large so that the plastic zone is contained within the domain and does not intersect with the right and bottom boundaries. An automatically adaptive mesh refinement technique in OptumG2 is used to improve the accuracy of upper and lower bound solutions [55]. Using this technique, the number of elements is automatically increased in the zone with high shear power dissipation that requires sensitivity analyses. The five iterations of the adaptive meshing are used in this study, where the number of elements is set to be automatically increased from 5000 to 10,000 elements [56–67].

The seismic bearing capacity of strip footing on a slope can be represented by dimensionless parameters [68] as follows:

$$N_c = \frac{q_u}{c_u} = f\left(\beta, \frac{H}{B}, \frac{L}{B}, \frac{D}{B}, \frac{c_u}{\gamma B}, k_h\right), \quad (1)$$

where N_c is the undrained seismic bearing capacity factor; q_u is the ultimate bearing capacity, H/B is the normalized slope height; L/B is the normalized distance from top slope to edge of the footing; D/B is the normalized depth of footing; $c_u/\gamma B$ is the strength ratio. k_h is the horizontal seismic acceleration. The seismic bearing capacity factor can be normalized as $N_c = q_u/c_u$ in Eq. (1). Numerical results are averaged values from UB and LB solutions of OptumG2. The study covers a range of five dimensionless parameters, which comprise the value of $c_u/\gamma B$ varies from 1.5 to 5.0, while H/B varies from 1 to 4, L/B values have the ranges of 0–4, D/B varies from 1 to 2, four β values of 15°, 30°, 45°, and 60° and the horizontal seismic acceleration coefficient k_h is taken into account at three distinct values of 0.1, 0.2, and 0.3, respectively. These ranges are decided based on the related published literature in [40–42].

Comparison of Results

The comparisons are for the investigations into the variation of N_c with k_h considering the changing angle slope β with a set of values of remaining dimensionless parameters of $c_u/\gamma B$, H/B, L/B. Figures 3, 4, 5 and 6 show such comparisons. A comparison of N_c variation is presented in Fig. 3 using the

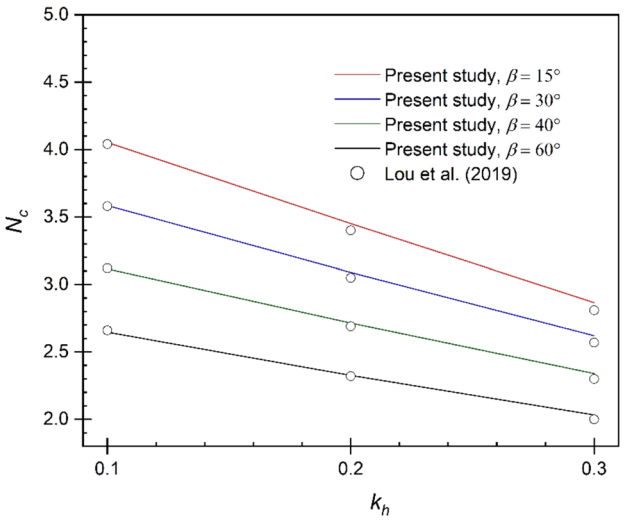

Fig. 3 Comparison of variation in N_c with k_h ($c_u/\gamma B = 5$, $D/B = 0$, $H/B = 4$, and $L/B = 0$)

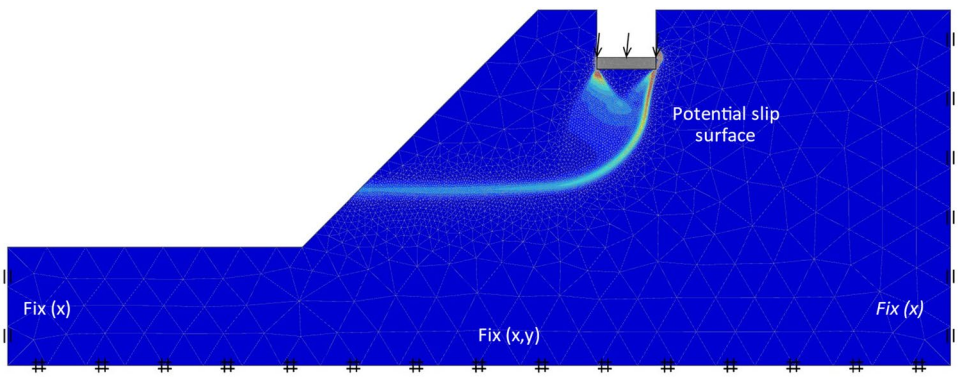

Fig. 2 Numerical model, boundary condition, and failure mechanism

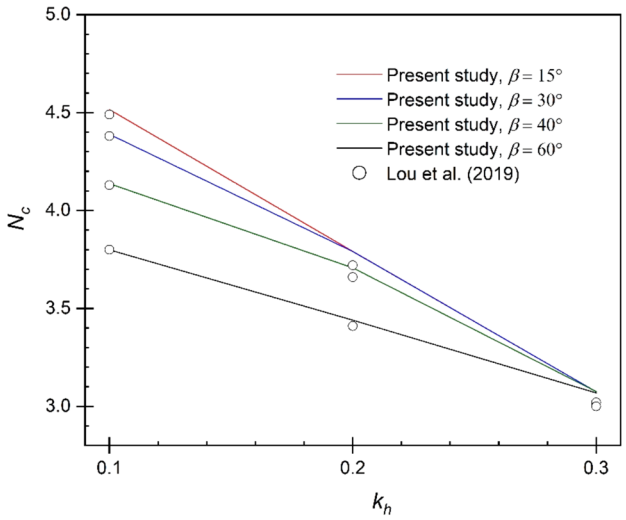

Fig. 4 Comparison of variation in N_c with k_h ($c_u/\gamma B = 5$, $D/B = 0$, $H/B = 4$, and $L/B = 1$)

case of ($c_u/\gamma B = 5$, $D/B = 0$, $H/B = 4$, and $L/B = 0$) for the four various slope angles. Also shown in Fig. 4 is for the case of $L/B = 1$. All other parameters are the same as in Fig. 3. In general, the bearing capacity factor N_c decreases linearly with increasing k_h. The numerical comparisons have shown that the present results are slightly larger than those lower bound results in Lou et al. [41], despite the fact that they are in good agreement. Seeing the results of $k_h = 0.3$ in Fig. 4, there is a tendency that all curves merge into one point, i.e., one N_c value. One possible reason may be due to the fact that the slopes become unstable as k_h increases, resulting in one small value of N_c. This comparison exercise has provided good confidence in producing all later parametric results in the paper.

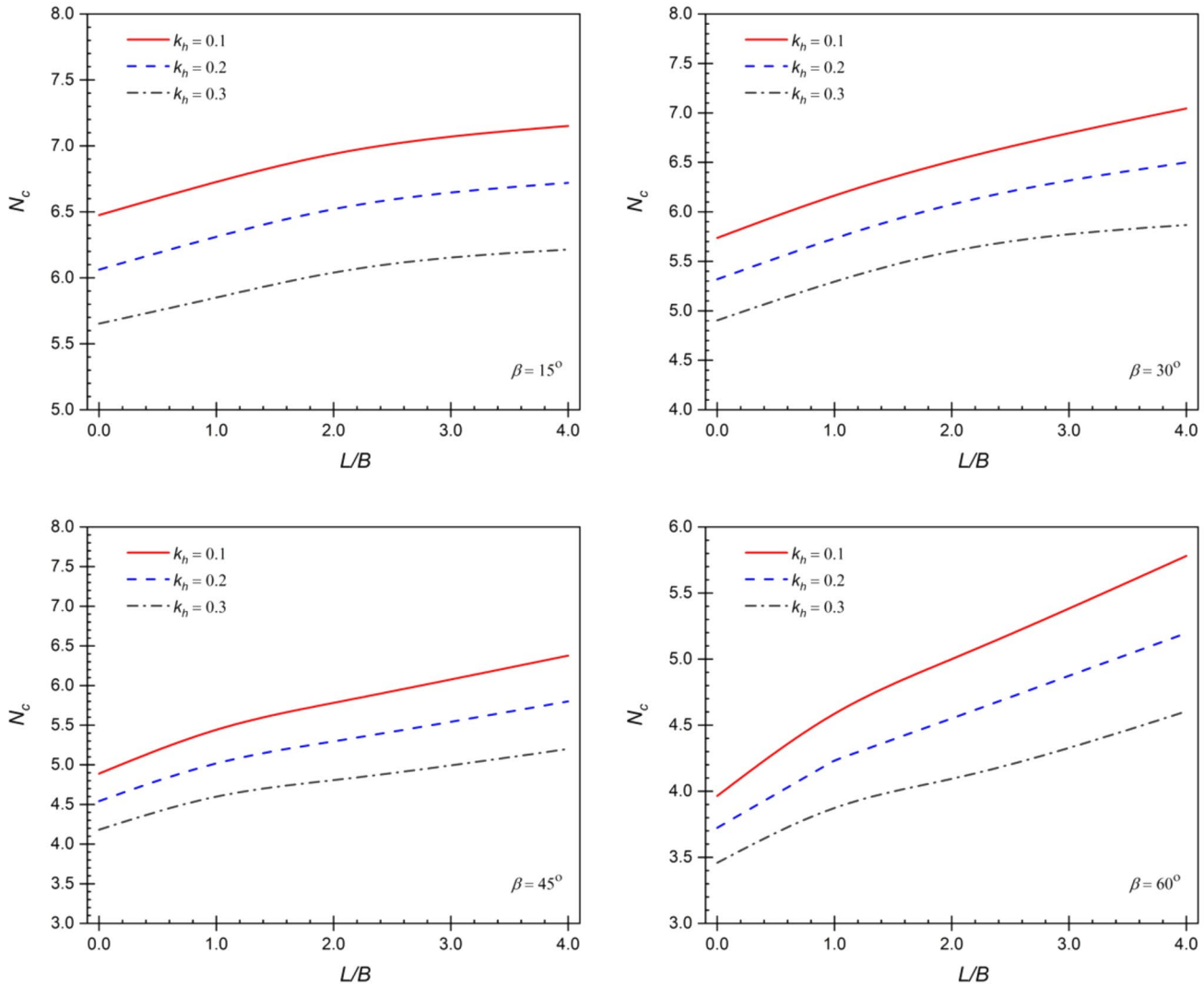

Fig. 5 Variation of N_c with L/B ($c_u/\gamma B = 2.5$, $H/B = 4$, and $D/B = 1$)

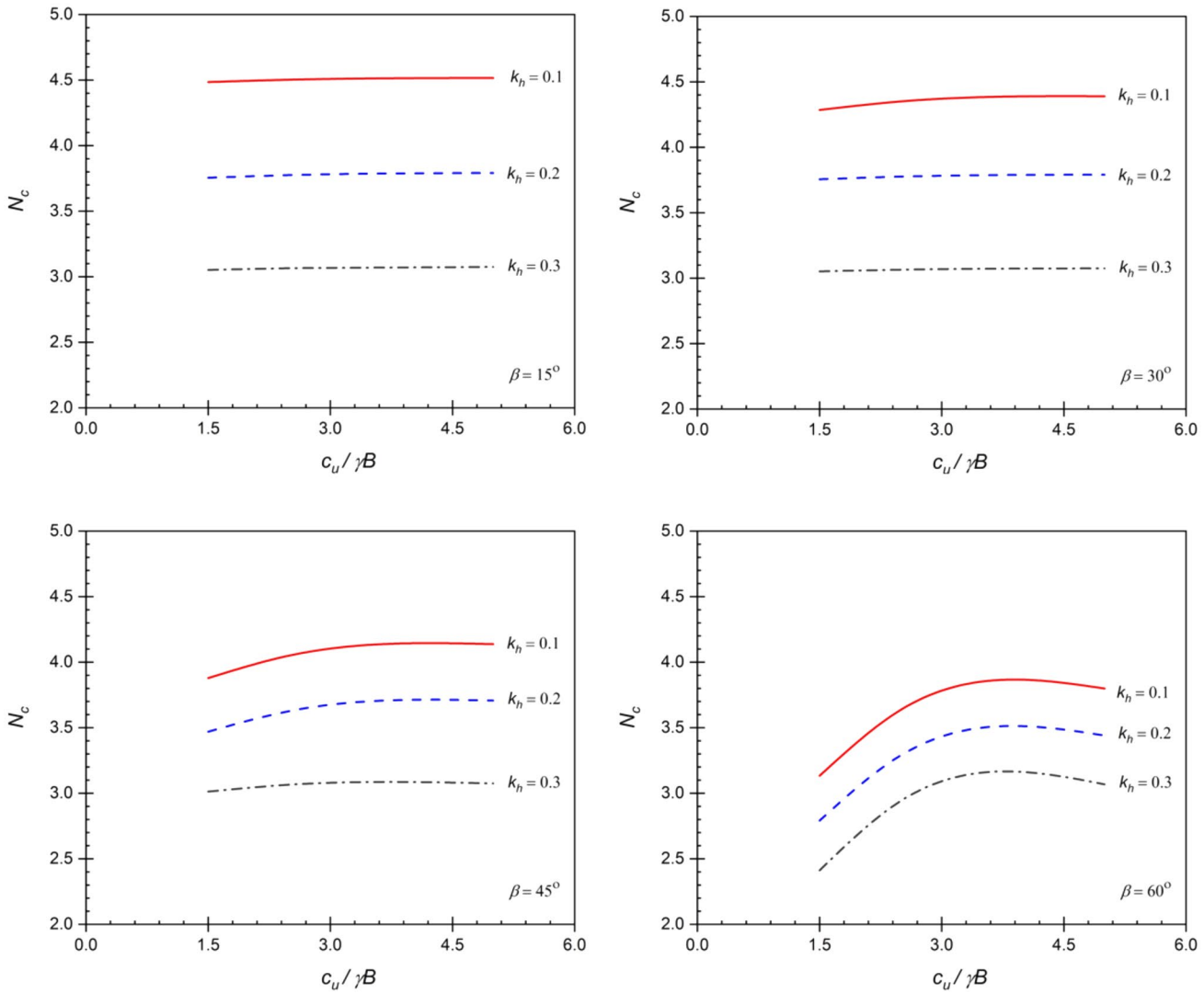

Fig. 6 Variation of N_c with $c_u/\gamma B$ ($L/B = 1$, $H/B = 4$, and $D/B = 0$)

Results and Discussion

The relationship between N_c and L/B for the various values of k_h and β is presented in Fig. 5 for the case of ($c_u/\gamma B = 2.5$, $H/B = 4$ and $D/B = 1$). Numerical results have shown that, for all values of k_h, the bearing capacity factor N_c increases nonlinearly with the increasing L/B. The larger the pseudo-static acceleration factor k_h, the less the value of N_c. The trend is the same for all slope angles β. Nevertheless, the rate of increase (gradient of line) is different from one to the other where the larger the slope angle, the greater the increase of N_c as L/B increases.

The variation study of N_c with $c_u/\gamma B$ is presented in Fig. 6 for the case of ($L/B = 1$, $H/B = 4$ and $D/B = 0$). Three values of k_h and four values of slope angles β are included in the study. For $\beta = 15°$ and 30°, the value of N_c is almost constant as the value of $c_u/\gamma B$ increases. However, the relationship between N_c and $c_u/\gamma B$ becomes nonlinear as β increases (see for example, $\beta = 45°$ and 60°). In particular, for $\beta = 60°$, the increase in N_c stops approximately at a value of $c_u/\gamma B = 3.5$, after which a slight decrease of N_c is attained. It can, therefore, be concluded that the effect of $c_u/\gamma B$ on N_c is conspicuous at a higher value of β. Numerical results have also shown that an increase of k_h or β leads to a decrease in N_c.

The next study is for the relationship between N_c and β. This is shown in Fig. 7 for three k_h values and four different values of L/B of the case ($c_u/\gamma B = 2.5$, $H/B = 4$ and $D/B = 1$). In general, N_c decreases as β increases for all values of L/B. The rate of decrease (gradient) becomes smaller as L/B increases, and the relationship between N_c and β becomes

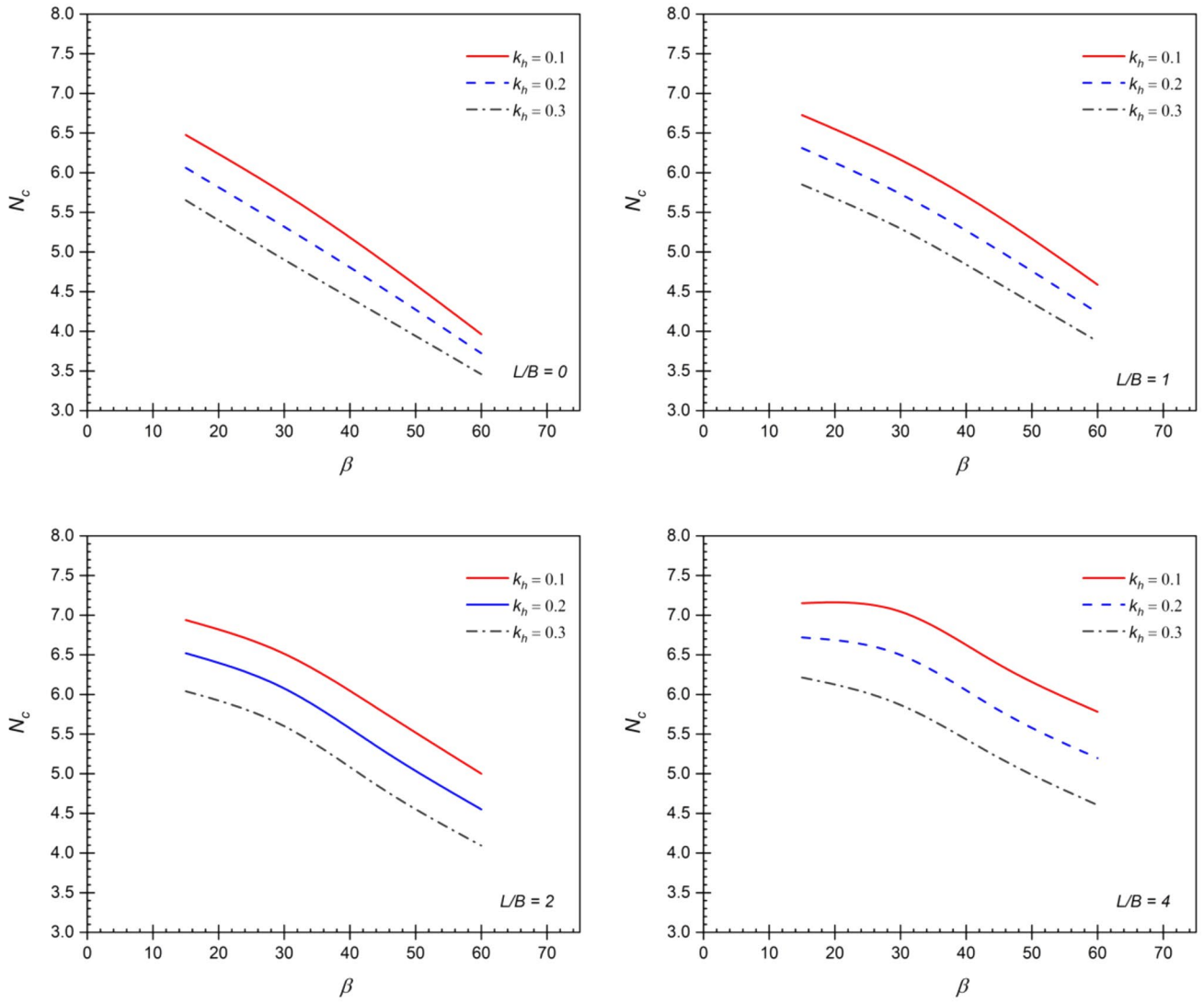

Fig. 7 Variation of N_c with β ($c_u/\gamma B = 2.5$, $H/B = 4$, and $D/B = 1$)

nonlinear. The results have also shown that an increase of k_h results in a decrease of N_c and an increase of L/B leads to an increase in N_c. Using the same data in Fig. 7, the figure presented in Fig. 8 shows the effect of k_h on N_c. As expected, the increase of k_h is to decrease the bearing capacity factor N_c. The relationship is a linear reduction, and the gradients of the lines are almost the same for all values of β and L/B.

The final study is for the variations of N_c with the normalized footing depth ratio D/B. This is presented in Fig. 9 using the case of ($c_u/\gamma B = 2.5$, $L/B = 1$ and $H/B = 4$). As D/B increases, so as the N_c. The relationship is a nonlinear one. This trend is similar to a standard bearing capacity problem of a shallow foundation. In addition, the smaller the slope angle β, the larger the bearing capacity factor N_c. The larger the k_h, the smaller the bearing capacity factor N_c.

All numerical results of the bearing capacity factor N_c corresponded to the investigated dimensionless input parameters are presented in Tables 1, 2 and 3. These data will be used for MARS study in a later section. In regard to the associated failure mechanisms, selected studies are presented in Figs. 10, 11 and 12 for the effects of $c_u/\gamma B$, D/B, and k_h, respectively.

The upper bound shear dissipation contour plots are normally used to represent failure mechanisms of geo-stability problems. The actual values of the colored contour are not important for a perfectly plasticity constitutive model, and, therefore, the contour bars for these plots are not normally shown in a technical document. Figure 10 shows the effects of $c_u/\gamma B$ on the associated failure mechanisms. The selected

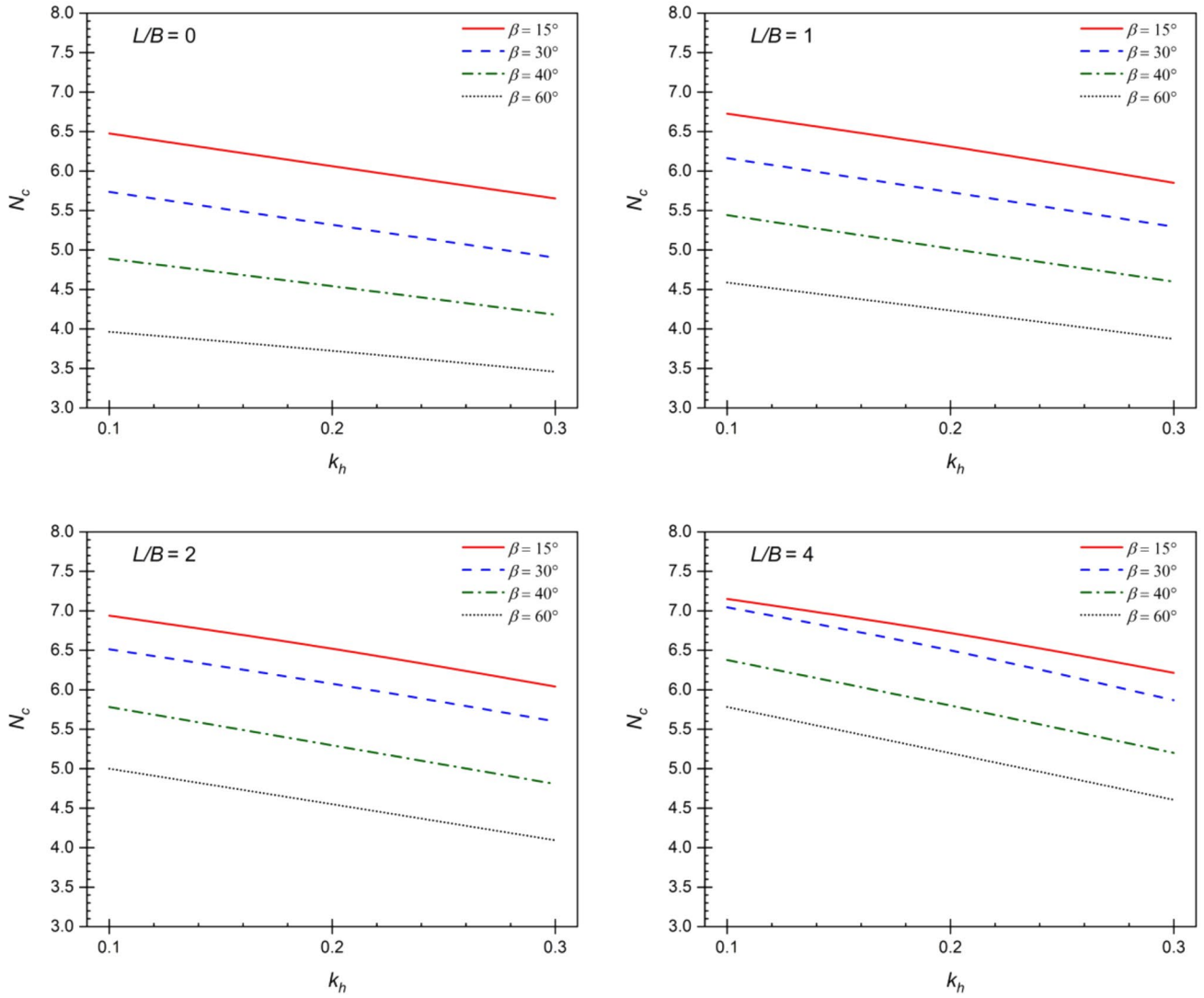

Fig. 8 Variation of N_c with k_h ($c_u/\gamma B = 2.5$, $H/B = 4$, and $D/B = 1$)

case is for ($\beta = 30°$, $L/B = 2$, $H/B = 4$, $D/B = 1$ and $k_h = 0.1$). Note that, as the value of $c_u/\gamma B$ increases, the overall area of the slip zone reduces, and the failure type transforms from a toe-failure mode to a face-failure mode. The reduction in the area of failure zone indicates an increase in seismic bearing capacity as the shear strength ratio $c_u/\gamma B$ of the soil slope increases.

The effect of D/B on the associated failure mechanisms is presented in Fig. 11. The selected case for this study is for ($\beta = 15°$, $c_u/\gamma B = 2.5$, $L/B = 0$, $H/B = 4$ and $k_h = 0.1$). The seismic bearing capacity increases as D/B increases, and there appears that the local failure mechanism is similar to a single sided Prandtl type of failures. For studying the effect of k_h on the associated failure mechanisms, the case of ($\beta = 30°$, $c_u/\gamma B = 2.5$, $L/B = 0$, $H/B = 4$ and $D/B = 1$) is chosen. This is shown in Fig. 12, where a slight decrease in the area of failure zone is depicted as the value of k_h increases. This makes sense, as the larger seismic forces would enable a search of the shortest path of the slip line to the slope surface, and, therefore, it leads to a decrease in the seismic bearing capacity, as well as a reduction in the area of the failure zone.

Sensitivity Study Using MARS Model

Multivariate adaptive regression splines (MARS) model is a nonlinear and non-parametric regression approach that can be used to capture nonlinear relationships between the input variables and the output results using a series of piecewise linear segments (splines) with differing gradients. The MARS technique does not require any specific assumptions to build functional correlations between the input variables and the output results. The different splines are connected using a knot representing by the end of one spline and the

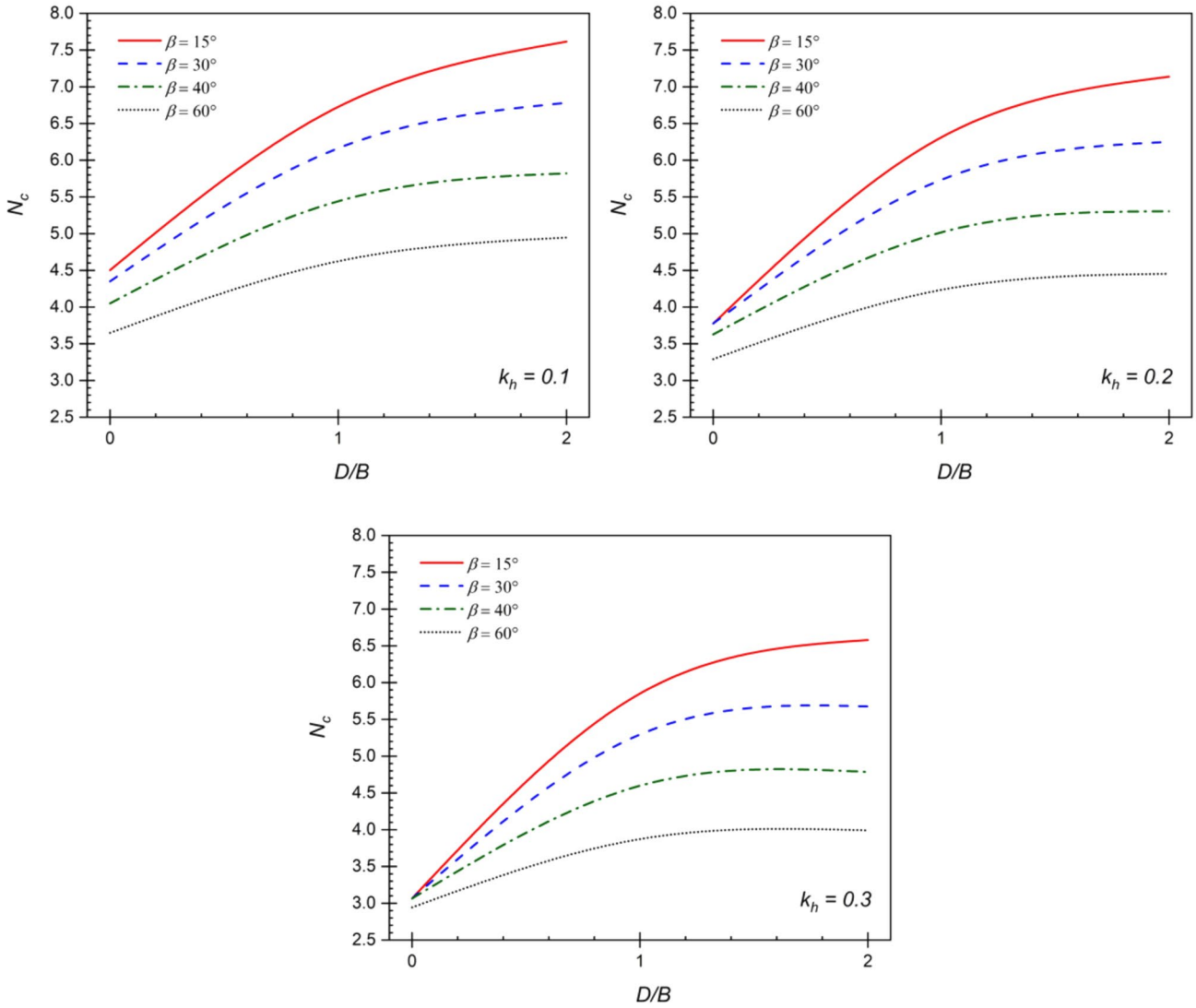

Fig. 9 Variation of N_c with D/B ($c_u/\gamma B = 2.5$, $L/B = 1$, and $H/B = 4$)

beginning of another. The fitted basic functions (BFs) have the flexibility to a studied model where the bends, thresholds, and other derivations from linear functions are allowed. The basic function can be generally written as in the following equation:

$$\mathrm{BF} = \max(0, x - t) = \begin{cases} x - t & \text{if } x > t \\ 0 & \text{otherwise} \end{cases}, \tag{2}$$

where x is an input variable and t is a threshold value.

MARS model produces BFs by searching in a stepwise manner, of which the knot locations will be automatically determined using the adaptive regression algorithm. MARS model is presented by a two-step procedure. The first (forward) step gives BFs and finds their potential knots to optimize the model performance and fitting accuracy. The second (backward) step uses pruning algorithm based on the generalized cross validation (GCV) value to delete the unimportant terms, leading to a final generation of an optimal model. The value of GVC can be determined by Eq. (3), where N indicates the number of basic functions, k indicates the penalty factor, RMSEi indicates the root mean square error for the training dataset, and R indicates the number of data points.

$$\mathrm{GCV} = \frac{\mathrm{RMSE}}{\left[1 - (N - kN)/R\right]^2} \tag{3}$$

To measure the important of each parameter on the output results, the value of relative important index (RII) would be

Table 1 Seismic bearing capacity N_c ($H/B = 1$)

β	D/B	k_h	$c_u/\gamma B$	L/B				β	D/B	k_h	$c_u/\gamma B$	L/B			
				0	1	2	4					0	1	2	4
15°	0	0.1	1.5	3.978	4.484	4.483	4.483	30°	0	0.1	1.5	3.464	4.287	4.483	4.483
			2.5	4.022	4.502	4.500	4.501				2.5	3.535	4.350	4.501	4.502
			5	4.052	4.515	4.514	4.515				5	3.585	4.389	4.515	4.514
		0.2	1.5	3.387	3.756	3.756	3.754			0.2	1.5	2.990	3.756	3.757	3.755
			2.5	3.424	3.776	3.776	3.770				2.5	3.049	3.775	3.776	3.774
			5	3.450	3.790	3.790	3.787				5	3.090	3.791	3.790	3.789
		0.3	1.5	2.826	3.052	3.052	3.052			0.3	1.5	2.550	3.053	3.052	3.052
			2.5	2.849	3.066	3.065	3.065				2.5	2.592	3.065	3.066	3.065
			5	2.866	3.075	3.075	3.075				5	2.620	3.076	3.075	3.075
	1	0.1	1.5	6.559	6.854	7.101	7.381		1	0.1	1.5	6.026	6.391	6.700	7.204
			2.5	6.476	6.731	6.939	7.151				2.5	5.978	6.303	6.596	7.080
			5	6.399	6.615	6.799	6.979				5	5.933	6.226	6.506	6.980
		0.2	1.5	6.066	6.344	6.578	6.895			0.2	1.5	5.532	5.868	6.166	6.638
			2.5	6.065	6.314	6.517	6.722				2.5	5.535	5.863	6.166	6.653
			5	6.030	6.249	6.430	6.591				5	5.531	5.853	6.147	6.590
		0.3	1.5	5.535	5.777	5.977	6.278			0.3	1.5	4.993	5.314	5.587	6.013
			2.5	5.615	5.850	6.041	6.215				2.5	5.079	5.411	5.701	6.155
			5	5.617	5.827	5.998	6.121				5	5.110	5.448	5.743	6.118
	2	0.1	1.5	7.825	8.012	8.184	8.476		2	0.1	1.5	7.606	7.825	8.001	8.283
			2.5	7.458	7.626	7.794	8.054				2.5	7.300	7.449	7.570	7.847
			5	7.177	7.329	7.472	7.701				5	7.058	7.142	7.233	7.515
		0.2	1.5	7.267	7.418	7.557	7.801			0.2	1.5	7.087	7.265	7.406	7.640
			2.5	6.997	7.151	7.304	7.559				2.5	6.856	6.986	7.090	7.350
			5	6.788	6.938	7.076	7.294				5	6.664	6.735	6.833	7.120
		0.3	1.5	6.629	6.742	6.842	7.009			0.3	1.5	6.495	6.629	6.729	6.903
			2.5	6.459	6.593	6.727	6.955				2.5	6.331	6.434	6.527	6.758
			5	6.312	6.453	6.578	6.779				5	6.184	6.240	6.349	6.623
45°	0	0.1	1.5	2.947	3.903	4.479	4.484	60°	0	0.1	1.5	2.437	3.545	4.290	4.485
			2.5	3.048	4.049	4.500	4.501				2.5	2.563	3.708	4.430	4.501
			5	3.116	4.136	4.516	4.516				5	2.646	3.821	4.513	4.515
		0.2	1.5	2.576	3.474	3.755	3.752			0.2	1.5	2.152	3.141	3.756	3.756
			2.5	2.659	3.627	3.776	3.774				2.5	2.257	3.321	3.776	3.775
			5	2.714	3.708	3.790	3.789				5	2.326	3.444	3.790	3.790
		0.3	1.5	2.233	3.049	3.052	3.052			0.3	1.5	1.890	2.769	3.052	3.053
			2.5	2.298	3.065	3.067	3.066				2.5	1.976	2.953	3.064	3.065
			5	2.340	3.075	3.074	3.074				5	2.033	3.068	3.076	3.075
	1	0.1	1.5	5.852	6.231	6.542	7.060		1	0.1	1.5	5.758	6.151	6.459	6.979
			2.5	5.835	6.126	6.418	6.933				2.5	5.767	6.049	6.321	6.841
			5	5.812	6.040	6.320	6.831				5	5.765	5.955	6.215	6.735
		0.2	1.5	5.395	5.703	5.995	6.503			0.2	1.5	5.323	5.632	5.912	6.423
			2.5	5.405	5.669	5.976	6.498				2.5	5.351	5.577	5.866	6.403
			5	5.397	5.637	5.946	6.475				5	5.365	5.532	5.825	6.375
		0.3	1.5	4.841	5.129	5.422	5.889			0.3	1.5	4.771	5.044	5.325	5.809
			2.5	5.405	5.202	5.508	6.011				2.5	4.861	5.092	5.391	5.918
			5	4.940	5.216	5.538	6.056				5	4.904	5.095	5.409	5.960

Table 1 (continued)

β	D/B	k_h	$c_u/\gamma B$	L/B				β	D/B	k_h	$c_u/\gamma B$	L/B			
				0	1	2	4					0	1	2	4
	2	0.1	1.5	7.516	7.748	7.942	8.216		2	0.1	1.5	7.461	7.701	7.906	8.183
			2.5	7.238	7.397	7.529	7.760				2.5	7.205	7.363	7.504	7.718
			5	7.025	7.112	7.184	7.416				5	7.006	7.095	7.171	7.363
		0.2	1.5	7.012	7.202	7.357	7.586			0.2	1.5	6.965	7.163	7.329	7.554
			2.5	6.802	6.942	7.047	7.264				2.5	6.771	6.915	7.031	7.223
			5	6.634	6.713	6.773	7.020				5	6.614	6.209	6.759	6.960
		0.3	1.5	6.436	6.586	6.690	6.859			0.3	1.5	6.397	6.555	6.669	6.833
			2.5	6.287	6.402	6.483	6.678				2.5	6.260	6.380	6.465	6.638
			5	6.156	6.215	6.281	6.522				5	6.142	6.209	6.258	6.465

determined by Eq. (4). This equation calculates the different in GCV values between the models before and after delete the unimportant terms [69, 70]

$$RII(i) = \frac{\Delta g(i)}{\max\{\Delta g(i), \Delta g(2), \Delta g(3), \ldots, \Delta g(n)\}}, \tag{4}$$

where Δg is the increase in GCV when ith parameter is deleted.

To demonstrate the complex relationship between input variables and output results, MARS proposed the correlation equation by merging all linear basic functions (BFs), as shown in Eq. (5), where a_0 is the constant, N is the number of BFs, g_n is the nth BF, a_n is the coefficient of g_n.

$$f(x) = a_o + \sum_{n=1}^{N} a_n g_n(X) \tag{5}$$

Compare to another machine learning approach (i.e., artificial neural networks (ANN), least-square support vector regression, extreme learning machine, Gaussian process regression [71–77]) MARS are considered as an effective approach [74, 78]. Moreover, MARS model has been successfully applied to a number of geotechnical applications (see, e.g., [79–93]). Further details of MARS model can be found in Zhang [94].

This aforementioned MARS model was utilized to perform sensitivity analyses of each input variables (i.e., *L/B, β, $c_u/\gamma B$, D/B, H/B,* and k_h) and an empirical prediction of N_c value introduced by considering the coupling effects of input variables. All FELA numerical results presented in Tables 1, 2 and 3 are used as the artificial training data for MARS model. In that, the sets of dimensionless variables (i.e., *L/B, β, $c_u/\gamma B$, D/B, H/B,* and k_h) and the corresponding N_c values are assigned as input data and target value in MARS model. Totally, 1296 data sets are used for MARS model.

In engineering practice, a careful design requires sensitivity analysis of each input variable [95, 96]. This is best presented through the relative importance index (RII) for the design output, i.e., the N_c values. As mentioned above, the value of RII shows the degree of influence, i.e., a RII of 100% indicates that the corresponding input variable has the most significant influence on the output N_c. Figure 13 shows the RII of each dimensionless parameter from MARS analysis. Numerical results have shown that the normalized embedded depth *D/B* has the greatest effect on seismic bearing capacity of footings placed on slope with a RII of 100%. This is followed by k_h, *H/B*, β, *L/B,* and $c_u/\gamma B$ with RII of 39.38%, 38.83%, 35.16%, 29.15%, and 23.24%, respectively. These results indicates that, for a general shallow foundation, the width and depth of the foundation is most important to determine bearing capacity. Although the present study considers the influence of other parameters, they cannot replace the most importance of width and depth of the shallow foundation. Moreover, this RII study has improved our understanding on the level of importance of each design parameter for the problem considered. The confidence level in practical design can, therefore, be enhanced greatly with these RII values.

Table 4 presents an empirical prediction equation provided by MARS model where the 30 BFs are listed. They can be written as in the following equation:

$$\begin{aligned} N_c = {} & 6.984 + 1.301 \times \mathrm{BF1} - 2.357 \times \mathrm{BF2} - 4.130 \\ & \times \mathrm{BF3} - 0.036 \times \mathrm{BF4} - 0.004 \times \mathrm{BF5} + 0.014 \\ & \times \mathrm{BF6} + 0.006 \times \mathrm{BF7} - 0.007 \times \mathrm{BF8} - 0.179 \\ & \times \mathrm{BF9} - 2.300 \times \mathrm{BF10} + 0.016 \times \mathrm{BF11} + 0.240 \\ & \times \mathrm{BF12} - 0.383 \times \mathrm{BF13} - 0.158 \times \mathrm{BF14} - 0.375 \\ & \times \mathrm{BF15} - 0.388 \times \mathrm{BF16} + 0.278 \times \mathrm{BF17} - 0.246 \\ & \times \mathrm{BF18} - 0.701 \times \mathrm{BF19} - 0.105 \times \mathrm{BF20} - 0.108 \\ & \times \mathrm{BF21} - 0.170 \times \mathrm{BF22} + 0.347 \times \mathrm{BF23} + 0.037 \\ & \times \mathrm{BF24} - 0.081 \times \mathrm{BF25} - 0.073 \times \mathrm{BF26} + 0.030 \\ & \times \mathrm{BF28} - 0.332 \times \mathrm{BF29} + 0.321 \times \mathrm{BF30}. \end{aligned} \tag{6}$$

Table 2 Seismic bearing capacity N_c ($H/B=2$)

β	D/B	k_h	$c_u/\gamma B$	L/B				β	D/B	k_h	$c_u/\gamma B$	L/B			
				0	1	2	4					0	1	2	4
15°	0	0.1	1.5	3.978	4.483	4.484	4.484	30°	0	0.1	1.5	3.463	4.287	4.484	4.483
			2.5	4.022	4.500	4.502	4.503				2.5	3.535	4.349	4.501	4.502
			5	4.052	4.515	4.514	4.516				5	3.586	4.390	4.515	4.515
		0.2	1.5	3.387	3.756	3.756	3.751			0.2	1.5	2.990	3.757	3.756	3.754
			2.5	3.425	3.776	3.776	3.774				2.5	3.049	3.776	3.776	3.774
			5	3.451	3.791	3.790	3.788				5	3.090	3.791	3.791	3.786
		0.3	1.5	2.825	3.052	3.053	3.052			0.3	1.5	2.550	3.052	3.053	3.052
			2.5	2.849	3.065	3.066	3.065				2.5	2.593	3.065	3.065	3.066
			5	2.866	3.074	3.075	3.075				5	2.620	3.075	3.075	3.075
	1	0.1	1.5	6.560	6.855	7.103	7.384		1	0.1	1.5	5.583	6.024	6.392	7.382
			2.5	6.476	6.729	6.940	7.154				2.5	5.736	6.164	6.513	7.152
			5	6.401	6.614	6.799	6.974				5	5.782	6.172	6.492	6.976
		0.2	1.5	6.064	6.342	6.576	6.858			0.2	1.5	5.083	5.452	5.768	6.857
			2.5	6.064	6.311	6.517	6.722				2.5	5.321	5.734	6.075	6.722
			5	6.029	6.246	6.430	6.589				5	5.405	5.811	6.136	6.589
		0.3	1.5	5.531	5.719	5.805	5.897			0.3	1.5	4.588	4.869	5.116	5.900
			2.5	5.613	5.845	6.043	6.215				2.5	4.901	5.294	5.604	6.215
			5	5.617	5.827	5.995	6.118				5	5.027	5.423	5.738	6.118
	2	0.1	1.5	7.642	7.873	8.080	8.442		2	0.1	1.5	6.733	7.096	7.406	8.411
			2.5	7.409	7.615	7.790	8.057				2.5	6.598	6.936	7.219	8.055
			5	7.161	7.328	7.472	7.701				5	6.480	6.778	7.040	7.702
		0.2	1.5	6.970	7.138	7.284	7.533			0.2	1.5	6.146	6.452	6.711	7.526
			2.5	6.949	7.141	7.302	7.560				2.5	6.144	6.459	6.723	7.559
			5	6.776	6.936	7.073	7.296				5	6.107	6.404	6.659	7.342
		0.3	1.5	6.263	6.352	6.367	6.379			0.3	1.5	5.545	5.775	5.965	6.326
			2.5	6.454	6.619	6.724	6.954				2.5	5.658	5.939	6.173	6.952
			5	6.348	6.493	6.576	6.778				5	5.692	5.974	6.209	6.779
45°	0	0.1	1.5	2.947	3.878	4.399	4.483	60°	0	0.1	1.5	2.437	3.291	3.898	4.485
			2.5	6.048	4.050	4.503	4.501				2.5	2.563	3.636	4.266	4.502
			5	3.116	4.136	4.515	4.516				5	2.646	3.801	4.475	4.514
		0.2	1.5	2.576	3.467	3.756	3.756			0.2	1.5	2.152	2.950	3.445	3.754
			2.5	2.658	3.626	3.776	3.773				2.5	2.257	3.291	3.776	3.776
			5	2.714	3.708	3.791	3.788				5	2.326	3.442	3.791	3.790
		0.3	1.5	2.233	3.051	3.053	3.052			0.3	1.5	1.890	2.622	3.009	3.046
			2.5	2.298	3.065	3.065	3.065				2.5	1.977	2.943	3.066	3.066
			5	2.340	3.075	3.075	3.075				5	2.033	3.069	3.075	3.075
	1	0.1	1.5	4.700	5.375	5.892	6.628		1	0.1	1.5	3.886	4.832	5.515	6.382
			2.5	4.935	5.581	6.034	6.703				2.5	4.133	5.084	5.684	6.458
			5	5.085	5.678	6.089	6.723				5	4.309	5.229	5.758	6.482
		0.2	1.5	4.290	4.831	5.273	5.943			0.2	1.5	3.577	4.324	4.900	5.698
			2.5	4.571	5.138	5.574	6.235				2.5	3.846	4.656	5.204	5.976
			5	4.746	5.303	5.727	6.369				5	4.033	4.855	5.372	6.120
		0.3	1.5	3.869	4.289	4.650	5.207			0.3	1.5	3.241	3.813	4.280	4.974
			2.5	4.189	4.695	5.105	5.722				2.5	3.535	4.221	4.728	5.467
			5	4.396	4.931	5.348	5.963				5	3.739	4.472	4.985	5.723

Table 2 (continued)

β	D/B	k_h	$c_u/\gamma B$	L/B				β	D/B	k_h	$c_u/\gamma B$	L/B			
				0	1	2	4					0	1	2	4
	2	0.1	1.5	6.307	6.760	7.119	7.672		2	0.1	1.5	6.016	6.557	6.958	7.527
			2.5	6.185	6.571	6.893	7.412				2.5	5.961	6.379	6.703	7.243
			5	6.078	6.404	6.698	7.191				5	5.891	6.191	6.487	7.009
		0.2	1.5	5.765	6.138	6.450	6.927			0.2	1.5	5.542	5.965	6.288	6.795
			2.5	5.715	6.079	6.389	6.887				2.5	5.517	5.869	6.185	6.714
			5	5.664	6.007	6.306	6.797				5	5.467	5.764	6.080	6.612
		0.3	1.5	5.204	5.499	5.741	6.098			0.3	1.5	5.016	5.335	5.592	6.098
			2.5	5.231	5.565	5.851	6.292				2.5	5.029	5.343	5.639	6.128
			5	5.239	5.576	5.869	6.326				5	5.005	5.320	5.632	6.145

Table 3 Seismic bearing capacity N_c ($H/B = 4$)

B	D/B	k_h	$c_u/\gamma B$	L/B				β	D/B	k_h	$c_u/\gamma B$	L/B			
				0	1	2	4					0	1	2	4
15°	0	0.1	1.5	3.978	4.484	4.482	4.483	30°	0	0.1	1.5	3.463	4.285	4.483	4.483
			2.5	4.021	4.502	4.502	4.501				2.5	3.536	4.350	4.502	4.501
			5	4.053	4.516	4.516	4.515				5	3.585	4.390	4.516	4.515
		0.2	1.5	3.386	3.755	3.755	3.756			0.2	1.5	2.990	3.756	3.756	3.757
			2.5	3.424	3.775	3.775	3.776				2.5	3.049	3.776	3.776	3.776
			5	3.451	3.791	3.790	3.789				5	3.090	3.790	3.790	3.791
		0.3	1.5	2.825	3.052	3.052	3.053			0.3	1.5	2.550	3.052	3.052	3.052
			2.5	2.849	3.066	3.065	3.065				2.5	2.593	3.065	3.065	3.065
			5	2.866	3.074	3.075	3.075				5	2.621	3.075	3.075	3.075
	1	0.1	1.5	6.027	6.854	7.101	7.361		1	0.1	1.5	5.541	5.697	5.876	6.273
			2.5	6.476	6.727	6.939	7.151				2.5	5.736	6.164	6.512	7.044
			5	6.394	6.616	6.798	6.978				5	5.781	6.169	6.492	6.980
		0.2	1.5	5.199	6.254	6.329	-			0.2	1.5	4.916	4.914	4.943	5.067
			2.5	6.062	6.311	6.520	6.720				2.5	5.319	5.732	6.075	6.499
			5	6.030	6.248	6.428	6.589				5	5.408	5.810	6.137	6.589
		0.3	1.5	3.965	5.112	5.068	-			0.3	1.5	4.269	4.076	3.915	-
			2.5	5.653	5.851	6.040	6.215				2.5	4.903	5.295	5.601	5.868
			5	5.616	5.823	5.995	6.117				5	5.024	5.423	5.740	6.119
	2	0.1	1.5	7.643	7.863	8.072	7.892		2	0.1	1.5	6.003	6.214	6.441	6.883
			2.5	7.404	7.616	7.791	8.059				2.5	6.460	6.783	7.042	7.484
			5	7.159	7.328	7.471	7.689				5	6.447	6.765	7.035	7.457
		0.2	1.5	6.726	6.831	6.929	-			0.2	1.5	5.222	5.268	5.342	5.467
			2.5	6.950	7.138	7.304	7.557				2.5	5.993	6.250	6.455	6.832
			5	6.779	6.937	7.077	7.296				5	6.083	6.393	6.659	7.071
		0.3	1.5	5.539	5.511	5.492	-			0.3	1.5	4.410	4.248	4.120	-
			2.5	6.416	6.579	6.722	6.810				2.5	5.504	5.677	5.824	6.088
			5	6.310	6.452	6.578	6.778				5	5.679	5.971	6.209	6.583

Table 3 (continued)

B	D/B	k_h	$c_u/\gamma B$	L/B				β	D/B	k_h	$c_u/\gamma B$	L/B			
				0	1	2	4					0	1	2	4
45°	0	0.1	1.5	2.947	3.879	4.080	4.476	60°	0	0.1	1.5	2.437	3.133	3.223	3.759
			2.5	3.047	4.051	4.498	4.501				2.5	2.563	3.637	4.233	4.501
			5	3.116	4.137	4.515	4.514				5	2.646	3.799	4.474	4.514
		0.2	1.5	2.575	3.469	3.486	3.666			0.2	1.5	2.152	2.791	2.725	2.965
			2.5	2.658	3.627	3.777	3.775				2.5	2.257	3.291	3.775	3.775
			5	2.714	3.707	3.791	3.790				5	2.326	3.440	3.792	3.790
		0.3	1.5	2.233	3.013	2.875	2.748			0.3	1.5	1.890	2.412	2.225	2.144
			2.5	2.298	3.065	3.066	3.066				2.5	1.976	2.943	3.066	3.066
			5	2.340	3.075	3.076	3.075				5	2.032	3.068	3.075	3.075
	1	0.1	1.5	4.400	4.575	4.827	5.448		1	0.1	1.5	3.449	3.542	3.839	4.695
			2.5	4.889	5.442	5.782	6.377				2.5	3.964	4.587	5.000	5.781
			5	5.079	5.660	6.070	6.698				5	4.224	5.052	5.543	6.236
		0.2	1.5	3.987	3.969	4.049	4.387			0.2	1.5	3.201	3.077	3.174	3.683
			2.5	4.542	5.017	5.296	5.801				2.5	3.723	4.233	4.551	5.197
			5	4.742	5.295	5.714	6.345				5	3.981	4.725	5.184	5.867
		0.3	1.5	3.563	3.359	3.254	3.223			0.3	1.5	2.943	2.623	2.511	2.620
			2.5	4.182	4.598	4.807	5.200				2.5	3.458	3.873	4.094	4.605
			5	4.397	4.928	5.342	5.941				5	3.712	4.378	4.826	5.477
	2	0.1	1.5	4.798	5.085	5.444	6.169		2	0.1	1.5	3.674	4.011	4.518	5.536
			2.5	5.420	5.822	6.190	6.821				2.5	4.358	4.908	5.430	6.276
			5	5.666	6.093	6.442	7.012				5	4.744	5.351	5.816	6.536
		0.2	1.5	4.227	4.325	4.507	4.945			0.2	1.5	3.302	3.403	3.676	4.351
			2.5	4.982	5.304	5.613	6.162				2.5	4.034	4.452	4.871	5.600
			5	5.294	5.717	6.063	6.611				5	4.446	4.977	5.407	6.121
		0.3	1.5	3.661	3.560	3.531	3.562			0.3	1.5	2.927	2.803	2.840	3.067
			2.5	4.549	4.784	5.018	5.458				2.5	3.703	3.991	4.301	4.896
			5	4.920	5.326	5.657	6.155				5	4.124	4.599	5.002	5.674

To validate the accuracy of the proposed MARS-based design equation, a comparison of N_c value between the Eq. (6) solutions and the actual FELA solutions (average of UB and LB solutions) are presented in Fig. 14. The comparison results have shown that both solutions are in a good agreement, where the coefficient of determination of R^2 is 92.21%. The comparison shows that the proposed MARS-based can be well applied with reasonable accuracy in practices.

Conclusions

This study has examined the seismic bearing capacity performance of a strip footing resting on undrained cohesive slopes using the robust finite element limit analysis with upper and lower bound theorems. The following conclusions are drawn based on the study.

1. The extended parametric studies for the individual dimensionless parameters, i.e., (L/B, β, $c_u/\gamma B$, D/B, H/B, and k_h) were performed. The bearing capacity factor N_c increases with a rise of (L/B, D/B, and $c_u/\gamma B$), while it decreases as the values of (β and k_h) decrease. Comprehensive results were reported in both graphical and tabular forms for design practices.
2. Based on MARS model, the results of sensitivity analyses showed that the normalized depth of footing D/B has the most influential effect on the seismic bearing capacity factor N_c with important index (RII) of 100%

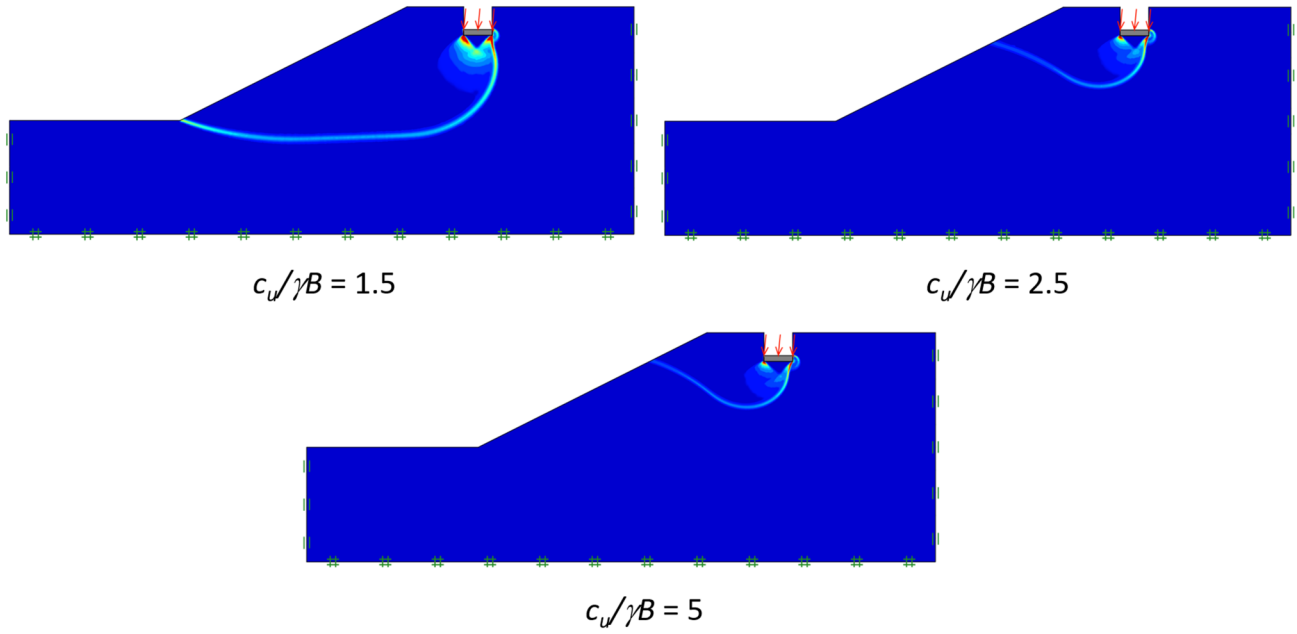

Fig. 10 Comparison of failure mechanisms ($\beta = 30°$, $L/B = 2$, $H/B = 4$, $D/B = 1$, and $k_h = 0.1$)

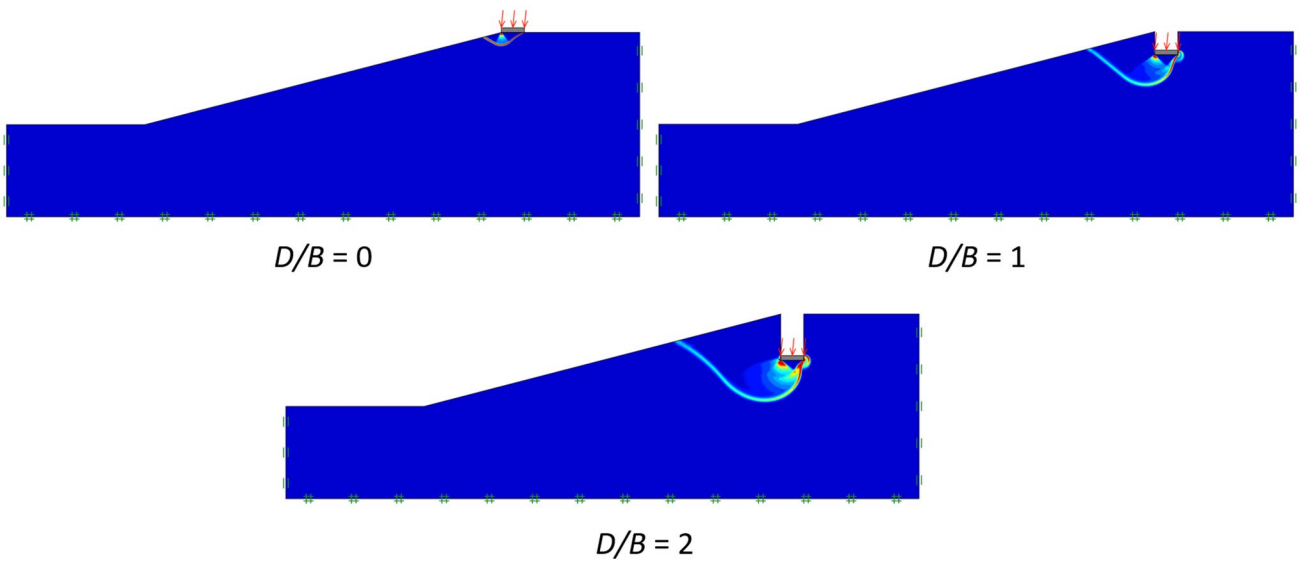

Fig. 11 Comparison of failure mechanisms for ($\beta = 15°$, $c_u/\gamma B = 2.5$, $L/B = 0$, $H/B = 4$, and $k_h = 0.1$)

while $c_u/\gamma B$ is the least importance parameter with RII of 23.24%. Other investigated parameters are followed by k_h, H/B, β, and L/B with RII of 39.38%, 38.83%, 35.16%, and 29.15%, respectively

3. An empirical equation with good accuracy ($R^2 = 92.21\%$) based on MARS model was proposed to determine the seismic bearing capacity factor N_c.

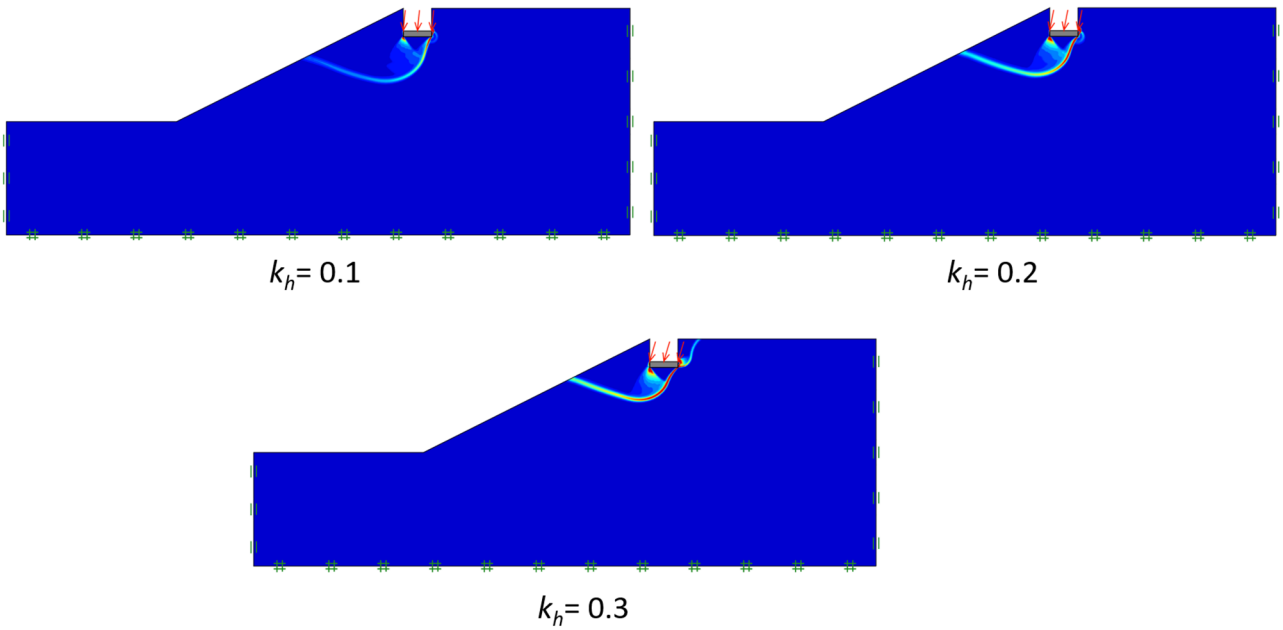

Fig. 12 Comparison of failure mechanisms for ($\beta = 30°$, $c_u/\gamma B = 2.5$, $L/B = 0$, $H/B = 4$, and $D/B = 1$)

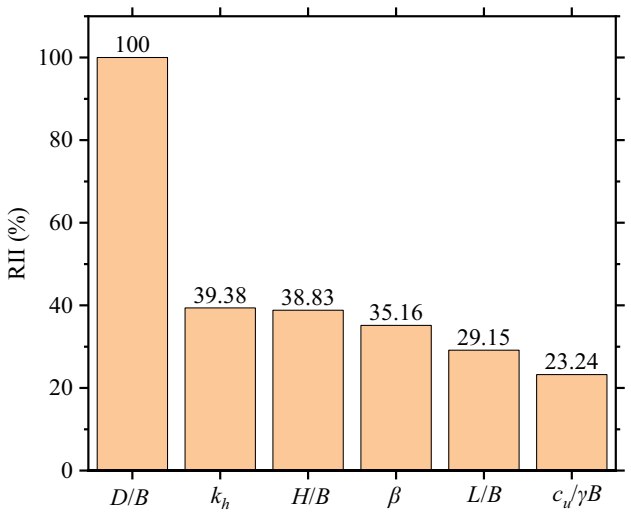

Fig. 13 Relative importance index of each input variable for the design N_c value

Table 4 Basis functions and mathematical equations in MARS model

BF	Equation	BF	Equation
BF1	max(0, $D/B-1$)	BF16	max(0, $H/B-1$)×BF3
BF2	max(1 − D/B, 0)	BF17	max(0, $L/B-2$)
BF3	max(0, $k_h-0.1$)	BF18	max(0, 2 − L/B)
BF4	max(0, $\beta-15$)	BF19	max(0, L/B)×BF3
BF5	max(0, $H/B-2$)×BF4	BF20	max(0, $H/B-2$)×BF17
BF6	max(0, 2 − H/B)×BF4	BF21	max(0, 2 − H/B)×BF17
BF7	max(0, $L/B-1$)×BF4	BF22	max(0, 2.5 − $c_u/\gamma B$)×BF17
BF8	max(0, 1 − L/B)×BF4	BF23	max(0, 2.5 − $c_u/\gamma B$)×BF2
BF9	max(0, $H/B-1$)×BF1	BF24	max(0, $k_h-0.1$)×BF4
BF10	max(0, 2.5 − $c_u/\gamma B$)×BF3	BF25	max(0, L/B)×BF1
BF11	max(0, 1 − D/B)×BF4	BF26	max(0, $c_u/\gamma B-1.5$)×BF1
BF12	max(0, $H/B-2$)×BF2	BF27	max(0, $H/B-1$)
BF13	max(0, 2 − H/B)×BF2	BF28	max(0, $c_u/\gamma B-2.5$)×BF27
BF14	max(0, $L/B-1$)×BF2	BF29	max(0, 2.5 − $c_u/\gamma B$)×BF27
BF15	max(0, 1 − L/B)×BF2	BF30	max(0, 2.5 − $c_u/\gamma B$)

$N_c = 6.984 + 1.301 \times BF1 - 2.357 \times BF2 - 4.130 \times BF3 - 0.036 \times BF4 - 0.004 \times BF5 + 0.014 \times BF6 + 0.006 \times BF7 - 0.007 \times BF8 - 0.179 \times BF9 - 2.300 \times BF10 + 0.016 \times BF11 + 0.240 \times BF12 - 0.383 \times BF13 - 0.158 \times BF14 - 0.375 \times BF15 - 0.388 \times BF16 + 0.278 \times BF17 - 0.246 \times BF18 - 0.701 \times BF19 - 0.105 \times BF20 - 0.108 \times BF21 - 0.170 \times BF22 + 0.347 \times BF23 + 0.037 \times BF24 - 0.081 \times BF25 — 0.073 \times BF26 + 0.030 \times BF28 - 0.332 \times BF29 + 0.321 \times BF30$

This study has paved the road for future geo-stability research to include sensitivity analysis of multi-variable problems with the useful relative importance index (RII) and design equation. This has many practical implications in the seismic design of soil structures in geotechnical engineering. However, it still has some limitations and should be investigated further in the future. For example, the proposed equation for the seismic bearing capacity factor N_c is appropriate for the ranges of dimensionless input parameters specified in the paper. The accuracy of the equation can be guaranteed if the input values are out

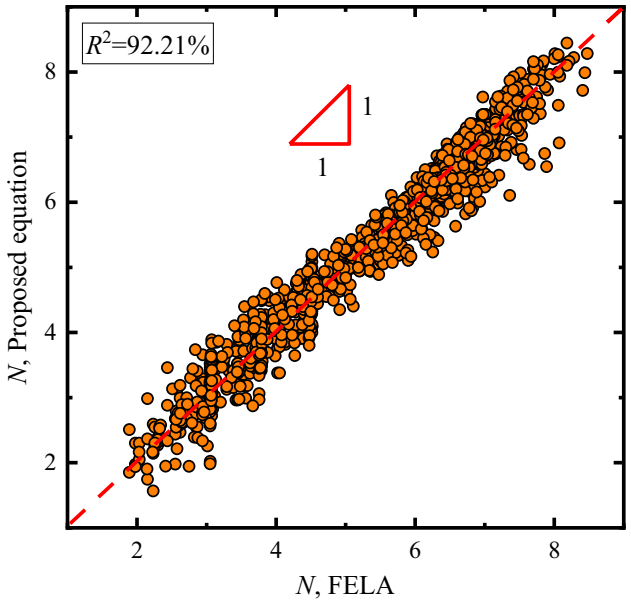

Fig. 14 Comparison of the N_c value between the proposed MARS equation and FELA

of these ranges. Besides, the present solutions cannot be used for multi-layered soils. Further research work can be expanded to study the layered effects.

Acknowledgements We would also like to thank Ho Chi Minh City University of Technology (HCMUT), VNU-HCM for the support of time and facilities for this study.

Author Contributions VQL and FL acquired methodology, software and contributed to investigation, conceptualization, writing—original draft and data curation. DY and WY acquired methodology, software and contributed to investigation, and data curation. JS provided resources, acquired supervision, contributed to writing—review and editing. SK acquired methodology, and contributed to investigation, conceptualization, writing—original draft.

Funding Open Access funding enabled and organized by CAUL and its Member Institutions.

Data Availability The data and materials in this paper are available.

Declarations

Conflict of Interest The authors declare that they have no conflicts of interest to this work.

References

1. Hansen B (1961) A general formula for bearing capacity. Danish Geotech Inst Bull 11:38–46
2. Satvati S, Alimohammadi H, Rowshanzamir M, Hejazi SM (2020) Bearing capacity of shallow footings reinforced with braid and geogrid adjacent to soil slope. Int J Geosynth Ground Eng 6(4):1–12
3. Khalvati Fahliani H, Arvin MR, Hataf N, Khademhosseini A (2021) Experimental model studies on strip footings resting on geocell-reinforced sand slopes. Int J Geosynth Ground Eng 7(2):1–15
4. Azzouz AS, Baligh MM (1983) Loaded areas on cohesive slopes. J Geotech Eng 109(5):724–729
5. Castelli F, Motta E (2010) Bearing capacity of strip footings near slopes. Geotech Geol Eng 28(2):187–198
6. Meyerhof G (1957) The ultimate bearing capacity of foundations on slopes. In: 4th International Conference on Soil Mechanics and Foundation Engineering, London
7. Narita K, Yamaguchi H (1990) Bearing capacity analysis of foudations on slopes by use of log-spiral sliding surfaces. Soils Foundations 30(3):144–152
8. Graham J, Andrews M, Shields D (1988) Stress characteristics for shallow footings in cohesionless slopes. Can Geotech J 25(2):238–249
9. Sokolovskii VVE (2016) Statics of granular media. Elsevier, New York
10. Davis E, Booker J (1973) Some adaptations of classical plasticity theory for soil stability problems. In: Published in the proceedings of the symposium on the role of plasticity in soil mechanics, September 13–15, 1973, Cambridge, England
11. Georgiadis K (2010) An upper-bound solution for the undrained bearing capacity of strip footings at the top of a slope. Géotechnique 60(10):801–806
12. Kusakabe O, Kimura T, Yamaguchi H (1981) Bearing capacity of slopes under strip loads on the top surfaces. Soils Found 21(4):29–40
13. Deng B, Yang M (2021) Bearing capacity analysis of submerged slopes subjected to water drawdown based on a nonassociated flow rule and nonlinear failure criteria. Bull Eng Geol Environ 80(2):835–850
14. Georgiadis K (2010) Undrained bearing capacity of strip footings on slopes. J Geotech Geoenviron Eng 136(5):677
15. Georgiadis K (2010) The influence of load inclination on the undrained bearing capacity of strip footings on slopes. Comput Geotech 37(3):311–322
16. Lai F, Chen F, Li D (2018) Bearing capacity characteristics and failure modes of low geosynthetic-reinforced embankments overlying voids. Int J Geomech 18(8):04018085
17. Nadaf MB, Mandal J (2017) Numerical analyses of loaded strip footing resting on cellular mattress and strips: reinforced fly ash slope. Int J Geosynth Ground Eng 3(3):1–16
18. Shiau J, Merifield R, Lyamin A, Sloan S (2011) Undrained stability of footings on slopes. Int J Geomech 11(5):381–390
19. Leshchinsky B (2015) Bearing capacity of footings placed adjacent to c′-ϕ′ slopes. J Geotech Geoenviron Eng 141(6):04015022
20. Leshchinsky B, Xie Y (2017) Bearing capacity for spread footings placed near c′-ϕ′ slopes. J Geotech Geoenviron Eng 143(1):06016020

21. Zhou H, Zheng G, Yin X, Jia R, Yang X (2018) The bearing capacity and failure mechanism of a vertically loaded strip footing placed on the top of slopes. Comput Geotech 94:12–21
22. Livaoğlu H, Irmak TS, Güven IT (2019) Seismic vulnerability indices of ground for Değirmendere (Kocaeli Province, Turkey). Bull Eng Geol Env 78(1):507–517
23. Zhang R, Xiao Y, Zhao M, Jiang J (2020) Seismic bearing capacity of strip footings placed near c-φ soil slopes. Soil Dyn Earthq Eng 136:106221
24. Goktepe F, Sahin M, Celebi E (2020) Small shaking table testing and numerical analysis of free-field site response and soil-structure oscillation under seismic loading. Bull Eng Geol Environ 79(6):2949–2969
25. Budhu M, Al-Karni A (1993) Seismic bearing capacity of soils. Geotechnique 43(1):181–187
26. Choudhury D, Subba RK (2006) Seismic bearing capacity of shallow strip footings embedded in slope. Int J Geomech 6(3):176–184
27. Kumar J, Kumar N (2003) Seismic bearing capacity of rough footings on slopes using limit equilibrium. Geotechnique 53(3):363–369
28. Farzaneh O, Mofidi J, Askari F (2013) Seismic bearing capacity of strip footings near cohesive slopes using lower bound limit analysis. In: 18th international conference on soil mechanics and geotechnical engineering, Paris
29. Askari F, Farzaneh O (2003) Upper-bound solution for seismic bearing capacity of shallow foundations near slopes. Geotechnique 53(8):697–702
30. Dormieux L, Pecker A (1995) Seismic bearing capacity of foundation on cohesionless soil. J Geotech Eng 121(3):300–303
31. Georgiadis K, Chrysouli E (2011) Seismic bearing capacity of strip footings on clay slopes. In: Proceedings of the 15th European Conference on Soil Mechanics and Geotechnical Engineering. IOS Press
32. Kumar J, Ghosh P (2006) Seismic bearing capacity for embedded footings on sloping ground. Geotechnique 56(2):133–140
33. Yamamoto K (2010) Seismic bearing capacity of shallow foundations near slopes using the upper-bound method. Int J Geotech Eng 4(2):255–267
34. Kumar J, Mohan RV (2003) Seismic bearing capacity of foundations on slopes. Geotechnique 53(3):347–361
35. Shiau JS, Lyamin AV, Sloan SW (2006) Application of pseudo-static limit analysis in geotechnical earthquake design. In: Proc., 6th European Conf. on Numerical Methods in Geotechnical Engineering. Taylor & Francis, London
36. Raj D, Singh Y, Shukla SK (2018) Seismic bearing capacity of strip foundation embedded in c-ϕ soil slope. Int J Geomech 18(7):04018076
37. Kumar J, Chakraborty D (2013) Seismic bearing capacity of foundations on cohesionless slopes. J Geotech Geoenviron Eng 139(11):1986–1993
38. Chakraborty D, Kumar J (2015) Seismic bearing capacity of shallow embedded foundations on a sloping ground surface. Int J Geomech 15(1):04014035
39. Chakraborty D, Mahesh Y (2016) Seismic bearing capacity factors for strip footings on an embankment by using lower-bound limit analysis. Int J Geomech 16(3):06015008
40. Cinicioglu O, Erkli A (2018) Seismic bearing capacity of surficial foundations on sloping cohesive ground. Soil Dyn Earthq Eng 111:53–64
41. Luo W, Zhao M, Xiao Y, Zhang R, Peng W (2019) Seismic bearing capacity of strip footings on cohesive soil slopes by using adaptive finite element limit analysis. Adv Civ Eng 2019:1–16
42. Beygi M, Keshavarz A, Abbaspour M, Vali R, Saberian M et al (2022) Finite element limit analysis of the seismic bearing capacity of strip footing adjacent to excavation in c-φ soil. Geomech Geoeng 17(1):246–259
43. Shiau J, Lyamin AV, Sloan SW (2004) Rigorous solution of classical lateral earth pressures. In: 6th Young Geotechnical Professionals Conference, Gold Coast, Australia, pp 162–167
44. Shiau J, Pather S, Ayers R (2006) Developing physical models for geotechnical teaching and research. In: Proc. 6th IC physical modelling in geotechnics, pp 157–162
45. Shiau J, Yu H (2000) Shakedown analysis of flexible pavements. In: Smith DW, Carter JP (eds) Proc. of the John Booker memorial symposium, pp 643–653
46. Shiau J, Lamb B, Sams M, Lobwein J (2017) Stability charts for unsupported circular tunnels in cohesive soils. Int J Geomate 13(39):95–102
47. Shiau J, Al-Asadi F (2020) Three-dimensional heading stability of twin circular tunnels. Geotech Geol Eng 38:2973–2988
48. Shiau J, Lee J-S, Al-Asadi F (2021) Three-dimensional stability analysis of active and passive trapdoors. Tunn Undergr Space Technol 107:103635
49. Abousnina RM, Manalo A, Shiau J, Lokuge W (2016) An overview on oil contaminated sand and its engineering applications. GEOMATE J 10(19):1615–1622
50. Abousnina RM, Shiau J, Manalo A, Lokuge W (2014) Effect of light hydrocarbons contamination on shear strength of fine sand, presented at the Fourth International Conference on Geotechnique, Construction Materials and Environment, Brisbane, Australia
51. Bhattacharya P, Shiau J, Barole S (2021) Improvement of bearing capacity of footings using reinforced granular trench. Int J Geosynth Ground Eng 7(79):1–14
52. Shiau J, Hassan MM (2021) Numerical investigation of undrained trapdoors in three dimensions. Int J Geosynth Ground Eng 7(2):1–12
53. Lai VQ, Keawsawasvong S, Shiau J (2022) Analysis of shaft-grouted piles using load-transfer method. Int J Geosynth Ground Eng 8(1):1–10
54. OptumG2 O (2020) Copenhagen, Denmark: Optum Computational Engineering. https://optumce.com/. Accessed 1 Dec 2020.
55. Ciria H, Peraire J, Bonet J (2008) Mesh adaptive computation of upper and lower bounds in limit analysis. Int J Numer Meth Eng 75(8):899–944
56. Keawsawasvong S, Lai VQ (2021) End bearing capacity factor for annular foundations embedded in clay considering the effect of the adhesion factor. Int J Geosynth Ground Eng 7(1):1–10
57. Keawsawasvong S, Ukritchon B (2020) Design equation for stability of shallow unlined circular tunnels in Hoek-Brown rock masses. Bull Eng Geol Environ 79:4167–4190
58. Ukritchon B, Yoang S, Keawsawasvong S (2019) Three-dimensional stability analysis of the collapse pressure on flexible pavements over rectangular trapdoors. Transport Geotech 21:100277
59. Yodsomjai W, Keawsawasvong S, Senjuntichai T (2021) Undrained stability of unsupported conical slopes in anisotropic clays based on Anisotropic Undrained Shear failure criterion. Transport Infrastruct Geotechnol 8(4):557–568
60. Ukritchon B, Yoang S, Keawsawasvong S (2020) Undrained stability of unsupported rectangular excavations in non-homogeneous clays. Comput Geotech 117:103281
61. Lai F, Chen S, Xue J, Chen F (2020) New analytical solutions for shallow cohesive soils overlying trench voids under various slip surfaces. Transport Geotech 25:100411
62. Chen F, Miao G, Lai F (2020) Base instability triggered by hydraulic uplift of pit-in-pit braced excavations in soft clay overlying a confined aquifer. KSCE J Civ Eng 24(6):1717–1730
63. Keawsawasvong S, Shiau J (2021) Instability of boreholes with slurry. Int J Geosynth Ground Eng 7(4):1–11
64. Yodsomjai W, Keawsawasvong S, Lai VQ (2021) Limit analysis solutions for bearing capacity of ring foundations on rocks

using Hoek-Brown failure criterion. Int J Geosynth Ground Eng 7(2):1–10
65. Lai VQ, Banyong R, Keawsawasvong S (2022) Stability of limiting pressure behind soil gaps in contiguous pile walls in anisotropic clays. Eng Fail Anal 134:106049
66. Lai VQ, Nguyen DK, Banyong R, Keawsawasvong S (2022) Limit analysis solutions for stability factor of unsupported conical slopes in clays with heterogeneity and anisotropy. Int J Comput Mater Sci Eng 11(1):2150030–2150128
67. Ukritchon B, Keawsawasvong S (2019) Design equations of uplift capacity of circular piles in sands. Appl Ocean Res 90:101844
68. Butterfield R (1999) Dimensional analysis for geotechnical engineers. Geotechnique 49(3):357–366
69. Gan Y, Duan Q, Gong W, Tong C, Sun Y et al (2014) A comprehensive evaluation of various sensitivity analysis methods: a case study with a hydrological model. Environ Model Softw 51:269–285
70. Steinberg D, Colla P, Martin K (1999) MARS user guide. Salford Systems, San Diego
71. Hasthi V, Raja MNA, Hegde A, Shukla SK (2022) Experimental and intelligent modelling for predicting the amplitude of footing resting on geocell-reinforced soil bed under vibratory load. Transport Geotech 100783
72. Khan MUA, Shukla SK, Raja MNA (2021) Soil–conduit interaction: an artificial intelligence application for reinforced concrete and corrugated steel conduits. Neural Comput Appl 33(21):14861–14885
73. Raja MNA, Shukla SK (2021) Predicting the settlement of geosynthetic-reinforced soil foundations using evolutionary artificial intelligence technique. Geotext Geomembr 49(5):1280–1293
74. Raja MNA, Shukla SK (2021) Multivariate adaptive regression splines model for reinforced soil foundations. Geosynth Int 28(4):368–390
75. Bardhan A, Biswas R, Kardani N, Iqbal M, Samui P et al (2022) A novel integrated approach of augmented grey wolf optimizer and ann for estimating axial load carrying-capacity of concrete-filled steel tube columns. Constr Build Mater 337:127454
76. Bardhan A, Kardani N, Alzo'ubi A K, Samui P, Gandomi AH et al (2022) A comparative analysis of hybrid computational models constructed with swarm intelligence algorithms for estimating soil compression index. Arch Comput Methods Eng 1–39
77. Bardhan A, Gokceoglu C, Burman A, Samui P, Asteris PG (2021) Efficient computational techniques for predicting the California bearing ratio of soil in soaked conditions. Eng Geol 291:106239
78. Wu L, Fan J (2019) Comparison of neuron-based, kernel-based, tree-based and curve-based machine learning models for predicting daily reference evapotranspiration. PLoS ONE 14(5):e0217520
79. Lai F, Zhang N, Liu S, Sun Y, Li Y (2021) Ground movements induced by installation of twin large diameter deeply-buried caissons: 3D numerical modeling. Acta Geotech 16(9):2933–2961
80. Zhang W, Goh ATC (2013) Multivariate adaptive regression splines for analysis of geotechnical engineering systems. Comput Geotech 48:82–95
81. Zhang W, Zhang Y, Goh AT (2017) Multivariate adaptive regression splines for inverse analysis of soil and wall properties in braced excavation. Tunn Undergr Space Technol 64:24–33
82. Zhang W, Zhang R, Goh AT (2018) MARS inverse analysis of soil and wall properties for braced excavations in clays. Geomech Eng 16(6):577–588
83. Zhang W, Zhang R, Wang W, Zhang F, Goh ATC (2019) A multivariate adaptive regression splines model for determining horizontal wall deflection envelope for braced excavations in clays. Tunn Undergr Space Technol 84:461–471
84. Zheng G, Zhang W, Zhou H, Yang P (2020) Multivariate adaptive regression splines model for prediction of the liquefaction-induced settlement of shallow foundations. Soil Dyn Earthq Eng 132:106097
85. Zheng G, Yang P, Zhou H, Zeng C, Yang X et al (2019) Evaluation of the earthquake induced uplift displacement of tunnels using multivariate adaptive regression splines. Comput Geotech 113:103099
86. Zhou H, Xu H, Yu X, Guo Z, Zheng G et al (2021) Evaluation of the bending failure of columns under an embankment loading. Int J Geomech 21(7):04021112
87. Goh A (2015) Nonlinear structural modeling using multivariate adaptive regression splines. Comput Concr Int J 16(4):569–585
88. Zhang W, Goh AT, Xuan F (2015) A simple prediction model for wall deflection caused by braced excavation in clays. Comput Geotech 63:67–72
89. Wang L, Wu C, Gu X, Liu H, Mei G et al (2020) Probabilistic stability analysis of earth dam slope under transient seepage using multivariate adaptive regression splines. Bull Eng Geol Env 79(6):2763–2775
90. Zhang W, Wu C, Li Y, Wang L, Samui P (2021) Assessment of pile drivability using random forest regression and multivariate adaptive regression splines. Georisk Assess Manag Risk Eng Syst Geohazards 15(1):27–40
91. Zhang W, Goh AT (2016) Multivariate adaptive regression splines and neural network models for prediction of pile drivability. Geosci Front 7(1):45–52
92. Sirimontree S, Jearsiripongkul T, Lai VQ, Eskandarinejad A, Lawongkerd J et al (2022) Prediction of penetration resistance of a spherical penetrometer in clay using multivariate adaptive regression splines model. Sustainability 14(6):3222
93. Jearsiripongkul T, Lai VQ, Keawsawasvong S, Nguyen TS, Van CN et al (2022) Prediction of uplift capacity of cylindrical caissons in anisotropic and inhomogeneous clays using multivariate adaptive regression splines. Sustainability 14(8):4456
94. Zhang W (2020) MARS applications in geotechnical engineering systems. Springer, Singapore
95. Zhang W, Wu C, Zhong H, Li Y, Wang L (2021) Prediction of undrained shear strength using extreme gradient boosting and random forest based on Bayesian optimization. Geosci Front 12(1):469–477
96. Zhang W, Li H, Han L, Chen L, Wang L (2022) Slope stability prediction using ensemble learning techniques: a case study in Yunyang County, Chongqing, China. J Rock Mech Geotech Eng